



What It Takes to Measure Reionization with Fast Radio Bursts

Stefan Heimersheim¹ , Nina S. Sartorio¹ , Anastasia Fialkov^{1,2} , and Duncan R. Lorimer^{3,4} ¹Institute of Astronomy, University of Cambridge, Madingley Road, Cambridge CB3 0HA, UK; heimersheim@ast.cam.ac.uk
²Kavli Institute for Cosmology, Madingley Road, Cambridge CB3 0HA, UK³West Virginia University, Department of Physics and Astronomy, P.O. Box 6315, Morgantown, WV, USA⁴Center for Gravitational Waves and Cosmology, West Virginia University, Chestnut Ridge Research Building, Morgantown, WV, USA

Received 2021 December 30; revised 2022 May 13; accepted 2022 May 16; published 2022 July 4

Abstract

Fast Radio Bursts (FRBs) are extragalactic radio transients that exhibit a distance-dependent dispersion of their signal, and thus can be used as cosmological probes. In this article we, for the first time, apply a model-independent approach to measure reionization from synthetic FRB data assuming these signals are detected beyond redshift 5. This method allows us to constrain the full shape of the reionization history as well as the CMB optical depth τ while avoiding the problems of commonly used model-based techniques. A total of 100 localized FRBs, originating from redshifts 5–15, could constrain (at 68% confidence level) the CMB optical depth to within 11%, and the midpoint of reionization to 4%, surpassing current state-of-the-art CMB bounds and quasar limits. Owing to the higher numbers of expected FRBs at lower redshifts, the τ constraints are asymmetric (+14%, –7%), providing a much stronger lower limit. Finally, we show that the independent constraints on reionization from FRBs will improve limits on other cosmological parameters, such as the amplitude of the power spectrum of primordial fluctuations.

Unified Astronomy Thesaurus concepts: [Reionization \(1383\)](#); [Radio transient sources \(2008\)](#); [Cosmology \(343\)](#)

1. Introduction

A type of radio transient signal, called Fast Radio Bursts (FRBs), is one of the unsolved mysteries in astronomy. The quest for understanding their origins is ongoing, and, since the discovery of the first FRB in 2007 (Lorimer et al. 2007), a few hundred such signals have been detected by the most sensitive radio telescopes.

These signals are significantly dispersed by the ionized medium distributed along the path between the sources and the observer. Since the observed dispersion, quantified by the dispersion measure (DM), is much larger than the contribution of our local environment, it is now known that the overwhelming majority of FRBs are of extragalactic origin. For the bulk of the detected FRBs, a large fraction of the DM is due to the free electrons found in the intergalactic medium (IGM; Xu & Han 2015), with a lesser contribution from the FRB host environment and the Milky Way. The evolution of the DM with the cosmological redshift of the FRB source may shed light on the properties of the IGM (Macquart et al. 2020) and can be used to measure cosmological parameters (Deng & Zhang 2014; Gao et al. 2014; Zhou et al. 2014; Yang & Zhang 2016; Walters et al. 2018; Jaroszynski 2019; Kumar & Linder 2019; Madhavacheril et al. 2019; Walters et al. 2019; Wu et al. 2020; Hagstotz et al. 2022).

Existing data suggest that the number of FRBs traces the star formation rate (SFR; Arcus et al. 2021; James et al. 2022), implying that FRBs could exist beyond the current observational cutoff at $z \sim 3$ (Bhandari et al. 2018). The expected relation between the SFR and the detection rate of high-redshift FRBs is uncertain as both the FRB luminosity function and the nature of FRB progenitors are poorly understood and might

change as stellar populations evolve. The recent detection of a Galactic FRB 200428 associated with magnetar SGR 1935 +2154 (Bochenek et al. 2020; The CHIME/FRB Collaboration et al. 2020) suggests that at least some FRBs are related to the highly magnetized neutron stars. However, even if all FRBs were produced by magnetars, the ambiguity remains as there are multiple channels through which a magnetar could give rise to an FRB (see, e.g., Popov & Postnov 2010; Petroff et al. 2016; Wadiasingh et al. 2020).

It is yet unknown when the first FRB-producing systems might have formed. Theoretical models predict an early onset of star formation with the first stars in the observable universe appearing just a few tens of million years after the Big Bang (Naoz et al. 2006). Additionally, observations of high-redshift galaxies find evolved and luminous objects, including a bright galaxy at $z \sim 11$ detected by the Hubble Space Telescope (HST; Oesch et al. 2016) and a metal-rich galaxy at $z \sim 9.1$ observed by the Atacama Large Millimeter/submillimeter Array, HST, and Spitzer, whose existence requires star formation to begin at $z \gtrsim 15$ (Hashimoto et al. 2018). Thus, if the correlation between SFR and the number of FRBs holds for the entirety of cosmic history, we can expect a multitude of FRBs produced in high-redshift galaxies (Fialkov & Loeb 2017; Hashimoto et al. 2020a). However, the number of these high-redshift events is expected to depend on the highly uncertain properties of the first stars and galaxies (e.g., the initial mass function of the first generation of stars; Klessen 2019).

From the observational point of view, detecting high-redshift FRBs requires both, sufficient telescope sensitivity and a capability to detect highly dispersed events. Some existing telescopes already have these specifications, including the Five-hundred-meter Aperture Spherical radio Telescope (FAST), which could detect the brightest FRBs up to $z \sim 10$ (Zhang 2018), and the Green Bank Telescope carrying out a high-sensitivity search using the GREENBURST experiment (Agarwal et al. 2020). Next-generation telescopes like the

Square Kilometre Array (SKA) will be able to detect multiple FRBs per day from high redshifts, potentially originating in the first billion years of cosmic history (Fialkov & Loeb 2016; Hashimoto et al. 2020b).

If detected, high-redshift FRBs will be extremely rewarding in terms of the science they deliver. First, either detection or nondetection of these events would probe progenitor theories and act as an indirect constraint on star formation at high redshifts. Second, high-redshift FRBs are expected to be sensitive cosmological probes, especially if accurate measurements of host galaxy redshift via source localization are available. Such capability already exists for the low-redshift FRBs observed with the Australian Square Kilometre Array Pathfinder (ASKAP; Bannister et al. 2019). Theoretical predictions show that a population of FRBs at $z \sim 3-4$ could be used to probe the second helium reionization happening around redshift $z \approx 3.5$ (Zheng et al. 2014; Linder 2020; Bhattacharya et al. 2021), while signals from $z > 5$ would primarily trace the ionization state of hydrogen atoms, and, consequently, could be used to probe the Epoch of Reionization (EoR; Fialkov & Loeb 2016; Beniamini et al. 2021; Dai & Xia 2021; Hashimoto et al. 2021; Pagano & Fronenberg 2021; Zhang et al. 2021). Such measurements would help constrain the history of reionization and the optical depth of the Cosmic Microwave Background (CMB), τ , to a higher accuracy than what is currently achievable (Fialkov & Loeb 2016; Beniamini et al. 2021; Dai & Xia 2021; Zhang et al. 2021).

Current best limits on τ have a large uncertainty ($\sim 13\%$; Planck Collaboration et al. 2020, hereafter referred to as Planck), and represent a hurdle for precision cosmology. These limits are derived from the CMB, which is affected by the EoR as photons scatter off the ionized gas. The signature of the EoR in the CMB is degenerate with the initial amplitude of curvature perturbations A_s (Hazra et al. 2018), and, thus, the poor precision in τ also degrades the estimates of the primordial power spectrum. Another quantity that suffers from the poor constraint of τ is the sum of neutrino masses, Σm_ν , extracted from a joint analysis of the CMB and Large Scale Structure (Brinckmann et al. 2019). Independent knowledge of the ionization history will also be important for 21 cm cosmology, breaking degeneracies between the ionization and thermal histories and allowing a measurement of the IGM temperature from the 21 cm signal (Fialkov & Loeb 2017). A more accurate measurement of the EoR history is therefore crucial to improve our fundamental understanding of the universe.

Existing works constraining hydrogen reionization based on localized FRBs (Fialkov & Loeb 2016; Beniamini et al. 2021; Hashimoto et al. 2021; Pagano & Fronenberg 2021; Zhang et al. 2021) make different assumptions that can either lead to biases in the results or limit the constraining power of the data, especially as our understanding and observations of FRBs and the IGM get better. Early studies (Fialkov & Loeb 2016) point out the relation between $DM(z)$ and $\tau(z)$, but do not consider multiple measurements distributed over redshift or the impact of the redshift-dependence of the ionized fraction ($x_i(z)$, also referred to here as the “shape” of the EoR history). Some recent analyses (one of the methods adopted in Beniamini et al. 2021; Hashimoto et al. 2021) consider constraining the ionized fraction by grouping FRBs into redshift bins and using the average DM in each bin. This allows measuring x_i between the bins but loses information about the redshifts and DMs of

individual FRBs, thus, limiting the resolution with which the reionization history can be traced. Furthermore, in the absence of a functional form for $x_i(z)$, this approach does not permit imposing global relationships such as monotonic evolution with redshift, or integrating over $x_i(z)$ to compute τ . A different approach is to postulate a specific shape of the reionization history, either using the popular tanh function (Zhang et al. 2021) or a simulation-based form (Pagano & Fronenberg 2021). Because the actual EoR history is unknown, however, assuming a specific history can lead to a significant offset in the results as we discuss in Section 6.

In this paper we, for the first time, use a free-form approach to estimate how well the EoR history can be probed with high-redshift FRBs (from $z > 5$), assuming these events are observed and localized with the future sensitive telescopes (e.g., the SKA). We use a free-form reionization parameterization, “FlexKnot” (Millea & Bouchet 2018), which allows us to constrain the full shape of the EoR history, thus yielding robust constraints on the optical depth τ . As this method does not assume a specific functional form for the reionization history, we can obtain a model-independent inference of τ and $x_i(z)$.

This paper is organized as follows: In Section 2 we briefly review different contributions to the observed FRB dispersion measure and discuss the associated uncertainties. In Section 3 we describe the synthetic data set of high-redshift FRBs, produced for this work. In Section 4 we present the model-independent method which is used to parameterize the EoR history. In Section 5 we outline the likelihood and inference procedure. The results are discussed in Section 6 where we show the FRB constraints on the full reionization history as well as on the values of the optical depth τ and other cosmological parameters. Finally we summarize our findings in Section 7.

2. Dispersion Measure

The DM of FRBs is commonly decomposed into three parts: contribution from free electrons in the IGM, the FRB host galaxy, and the Milky Way

$$DM = DM^{\text{IGM}} + DM^{\text{host}} + DM^{\text{MW}}. \quad (1)$$

We compute each one of these contributions as specified below, model the uncertainty of each component and, in addition, account for observational errors. Approximating the components as statistically independent Gaussian random variables, we add the uncertainties in quadrature

$$\sigma_{\text{DM}} = \sqrt{(\sigma_{\text{DM}}^{\text{IGM}})^2 + (\sigma_{\text{DM}}^{\text{host}})^2 + (\sigma_{\text{DM}}^{\text{MW}})^2 + (\sigma_{\text{DM}}^{\text{obs}})^2}. \quad (2)$$

2.1. IGM Contribution

The largest and the most important contribution to the dispersion of high-redshift FRBs is DM^{IGM} . Owing to the fluctuations in electron density along the line of sight, this quantity is stochastic with the distribution approaching a Gaussian (Macquart et al. 2020), as demonstrated by studies of the DM derived from numerical simulations (Jaroszynski 2019; Batten et al. 2021; Zhang et al. 2021). For FRBs originating from redshift z , the mean IGM contribution is given by

considering a homogeneous distribution of matter (electrons)

$$\overline{\text{DM}}^{\text{IGM}}(z) = \int_0^z \frac{c\bar{n}_e(z')}{H(z')(1+z')^2} dz' \quad (3)$$

where $\bar{n}_e(z')$ is the mean number density of free electrons at redshift z' , c is the speed of light, and $H(z')$ is the Hubble expansion rate. In order to explicitly compare the contributions due to reionization and other cosmological parameters we can separate the terms as

$$\begin{aligned} \overline{\text{DM}}^{\text{IGM}}(z) &= \frac{3c}{8\pi Gm_p} \int_0^z \underbrace{(1 + f_{\text{He}})x_i(z) + f_{\text{He}}x_i^{\text{He II}}(z)}_{\text{Reionization history}} \\ &\times \underbrace{\frac{\Omega_b H_0 (1+z')}{\sqrt{\Omega_m (1+z')^3 + (1-\Omega_m)}}}_{\text{Background cosmology}} dz' \end{aligned} \quad (4)$$

where we wrote $H(z)$ and $\bar{n}_e(z)$ in terms of the Hubble constant H_0 , the matter density parameter Ω_m , the physical baryon density parameter $\Omega_b H_0^2$, the gravitational constant G , the proton mass m_p , and the number of helium relative to hydrogen atoms f_{He} . We also introduced the ionized fractions $x_i^{\text{He II}}$ for the second helium reionization (occurring at $z=3-4$), and $x_i(z)$ quantifying the hydrogen (and first helium) reionization. At the high redshifts of interest ($z>5$), the integrand only depends on $x_i(z)$ and a factor proportional to $\Omega_b H_0 / \Omega_m^{-0.5}$.

Note that FRBs actually probe the electron density in the IGM, which is slightly lower than the mean cosmic density $\bar{n}_e(z)$ due to the contribution of electrons in stars and black holes. This discrepancy is usually mitigated by introducing a factor f_{IGM} , the fraction of electrons in the IGM, which plays an important role in cosmological studies with low-redshift FRBs (and causes a fixed offset of the DM value for $z>5$ FRBs). However, at high redshifts this fraction is close to unity, as was shown by Takahashi et al. (2021) in a simulation-based study. The authors find $f_{\text{IGM}} > 0.98$ at $z > 5$ and $f_{\text{IGM}} > 0.996$ at $z > 10$. Assuming $f_{\text{IGM}} = 1$ at $z > 5$ leads to a negligible error ($<1\%$) on τ .

We estimate the uncertainty on DM^{IGM} using the popular low-redshift ($z < 3$) relation (Kumar & Linder 2019)

$$\sigma_{\text{DM}}^{\text{IGM}}(z) = (0.2/\sqrt{z})\overline{\text{DM}}^{\text{IGM}} \quad (5)$$

derived from simulations (Jaroszyński 2020) which we extend to higher redshifts. We extrapolate the relation to the maximum uncertainty at $z_{\text{peak}} \approx 6.5$ and then assume this value for $z > z_{\text{peak}}$, i.e., we use Equation (5) with $\sigma_{\text{DM}}^{\text{IGM}}(z > z_{\text{peak}}) = \sigma_{\text{DM}}^{\text{IGM}}(z_{\text{peak}})$. Such treatment has been employed previously by Hashimoto et al. (2021), albeit with a fixed $z_{\text{peak}} = 6$. We note that if Equation (5) were revised in the future with new observations or simulations becoming available, the numerical value of the uncertainty in DM would, naturally, be affected. However, such a change would not have an impact on a comparative analysis of statistical methods, such as the one laid out here.

2.2. Galactic Contributions

The contributions to the total DM by the FRB host galaxy and the Milky Way are expected to be small compared to that of the IGM, which is $\gtrsim 4500 \text{ pc cm}^{-3}$ for the bursts produced at high redshifts $z > 5$.

The host contribution is not well determined (e.g., Tendulkar et al. 2017, found $55 \lesssim \text{DM}_{\text{host}} \lesssim 225$), and different values are used in the literature. Conservatively, we adopt a rather large uncertainty of $\sigma_{\text{DM}}^{\text{host}} = 100 \text{ pc cm}^{-3}$ (following Dai & Xia 2021) in the host galaxy rest frame.

The Milky Way contribution ($\lesssim 500 \text{ pc cm}^{-3}$ for samples in the CHIME/FRB catalog; Rafiei-Ravandi et al. 2021) can be estimated from Galactic electron models for every line of sight (Cordes & Lazio 2002; Yao et al. 2017) and subtracted from the DM measurement, thus it will not have a large impact when estimating the cosmological contribution of the high-redshift FRBs. We assume a 20 pc cm^{-3} modeling uncertainty, motivated by the average difference between NE2001 (Cordes & Lazio 2002) and YMW217 (Yao et al. 2017) models in the CHIME/FRB catalog. To account for the uncertain Milky Way halo contribution (Yamasaki & Totani 2020; Keating & Pen 2020; Das et al. 2021) we add an error of 50 pc cm^{-3} . Thus, with the errors combined in quadrature we obtain $\sigma_{\text{DM}}^{\text{MW}} \approx 54 \text{ pc cm}^{-3}$.

2.3. Measurement Uncertainty

The final uncertainty on the DM is the measurement error $\sigma_{\text{DM}}^{\text{obs}}$, which quantifies the accuracy of the FRB arrival time at different frequencies. To calculate the uncertainty we follow Lorimer et al. (2013), which gives

$$\sigma_{\text{DM}}^{\text{obs}} = \frac{\nu^3 T_{\text{sys}}}{k G s} \sqrt{\frac{W}{2\Delta\nu^3}} \quad (6)$$

where ν is the observed frequency, $\Delta\nu$ is the bandwidth, W is the observed pulse width, G is the instrumental gain, T_{sys} is the system temperature, s is the peak spectral flux density of the signal, and k is a constant $k = 4.15 \text{ GHz}^2 \text{ ms cm}^3 \text{ pc}^{-1}$ (e.g., Kulkarni 2020). In other words, $\sigma_{\text{DM}}^{\text{obs}}$ is mainly determined by the observed pulse width and the signal-to-noise ratio depending on the peak spectral flux density of the signal as well as on the instrumental parameters (Condon & Ransom 2016).

The observed pulse width is set by two factors: the intrinsic rest-frame width of an FRB, W_{int} , taken to be 1 ms, and a contribution due to dispersion smearing (the latter is small, $\lesssim 10\%$) and is given by

$$W = \sqrt{[W_{\text{int}}(1+z)]^2 + (\text{DM } k\Delta\nu / N_{\text{chan}}\nu^3)^2} \quad (7)$$

where z is the redshift of the FRB host galaxy, N_{chan} is the number of channels and DM is the total dispersion measure.⁵ Note that the sampling and scattering times are $\lesssim 10$ ms and, thus, are negligible for high-redshift FRBs.

For our analysis we use the most distant (at the time of writing) localized FRB, FRB180924 (Bannister et al. 2019), as a proxy for the peak spectral flux density s . We scale the peak flux value to higher host galaxy redshifts accounting for the luminosity distance and the spectral shape and assuming spectral index $\alpha = -1.5$ compatible with the recent results of CHIME/FRB (Rafiei-Ravandi et al. 2021). For comparison, FRB180924 has a higher intrinsic luminosity than about 75%

⁵ The total dispersion measure is dominated by the IGM contribution ($4500-6000 \text{ pc cm}^{-3}$, depending on redshift and the reionization history) and its scatter. To make sure the other contributions have a negligible effect on the dispersion smearing we add $(500 + 50 + 200) \text{ pc cm}^{-3}$ as conservative estimates of Milky Way ($\lesssim 500 \text{ pc cm}^{-3}$ for the sample in the CHIME/FRB catalog), halo (Yamasaki & Totani 2020), and host galaxy (Tendulkar et al. 2017) contributions, respectively.

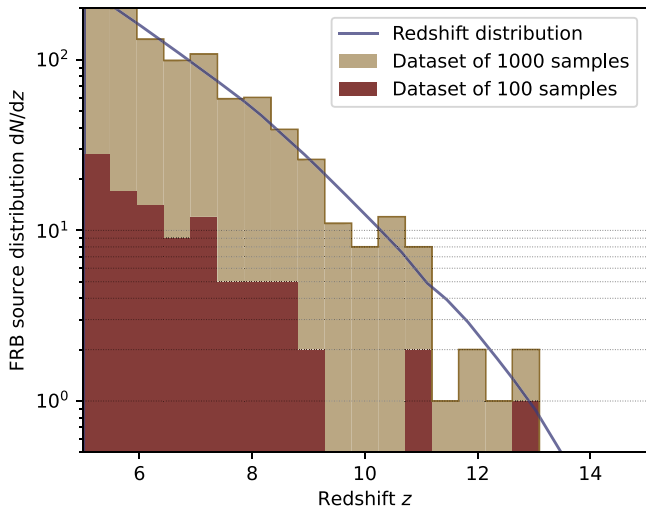


Figure 1. Source redshift samples for 100 and 1000 FRBs used in the analysis (histograms), compared to the analytical distribution (line plot) following SFR. The source redshifts are sampled from this distribution using a simple Monte Carlo rejection sampling.

of the CHIME/FRB catalog samples. The instrument parameters are taken to be similar to FAST (Nan et al. 2011) with $G = 15 \text{ K Jy}^{-1}$, $T_{\text{sys}} = 35 \text{ K}$, $\nu = 1.4 \text{ GHz}$, $\Delta\nu = 400 \text{ MHz}$, and $N_{\text{chan}} = 4096$. For completeness we take this uncertainty into account but its effect is mostly negligible, contributing $\sigma_{\text{DM}}^{\text{obs}} \lesssim 100 \text{ pc cm}^{-3}$.

3. Synthetic Data Set

We create a synthetic data set of high-redshift FRBs in order to demonstrate the potential of these sources in constraining the EoR. We generate two data sets, one with 100 and the other with 1000 localized FRBs. Each data set consists of the host galaxy redshifts z^{obs} generated from a distribution proportional to SFR, and dispersion measures DM^{obs} calculated following the prescription outlined in Section 2.

As we are interested in the EoR constraints, we consider host galaxies in the redshift range $z^{\text{true}} = 5\text{--}15$. We draw these true source redshifts from a distribution scaling with the cosmic SFR, adopting a fit from Behroozi et al. (2019), as shown in Figure 1. This choice is rather pessimistic, allowing for few $z > 10$ FRBs as the adopted SFR drops steeply at high redshifts. Concretely we find that we sample 85% of FRB sources between redshift $z^{\text{true}} = 5$ and 8, 12% between 8 and 10, 3% between 10 and 15, and no sources beyond $z^{\text{true}} > 15$. However, as mentioned in Section 1, the high-redshift star formation is not well constrained and a much higher SFR during the early stages of the EoR is plausible. A more efficient star formation at high redshifts would result in a larger number of FRBs and, thus, even stronger EoR constraints than what we report here, while a lower SFR would imply fewer FRBs and, consequently, weaker constraints. The method presented in this paper is generic and can be applied to an arbitrary SFR.

After generating the true host galaxy redshifts we simulate the observed redshifts z^{obs} , assuming an accuracy of 10% (such as provided by spectra of host galaxies from the James Webb Space Telescope), and draw z^{obs} from a Gaussian distribution $\mathcal{N}(\mu_z = z^{\text{true}}, \sigma_z = 0.1z^{\text{true}})$.

Finally we simulate the corresponding synthetic DM observations, DM^{obs} , by adding the IGM, Milky Way, and host galaxy contributions, and taking the associated

Table 1
FRB Constraints on Characteristic Points of the Reionization History

Quantity	100 FRBs			1000 FRBs		
	\hat{P}	68%	95%	\hat{P}	68%	95%
$x_i = 0.1$	$z = 7.8$	+0.9 -0.8	+3.8 -1.1	$z = 8.5$	+1.2 -0.8	+4.1 -1.1
$x_i = 0.5$	$z = 7.0$	+0.3 -0.3	+0.6 -0.6	$z = 7.2$	+0.1 -0.3	+0.3 -0.6
$x_i = 0.9$	$z = 6.1$	+0.5 -0.4	+0.9 -0.7	$z = 6.1$	+0.4 -0.2	+0.6 -0.5
τ	0.0510	+0.0071 -0.0036	+0.0187 -0.0058	0.0548	+0.0061 -0.0034	+0.0150 -0.0048
$\tau_{\text{w/o CMB}}$	0.0506	+0.0085 -0.0042	+0.0363 -0.0053	0.0537	+0.0103 -0.0034	+0.0261 -0.0039

Note. The start ($x_i = 0.1$), midpoint ($x_i = 0.5$), and end ($x_i = 0.9$) of the EoR. We also show the FRB constraint on the total CMB optical depth τ with and without the CMB constraint on $\tau_{15,30}$ (Heinrich & Hu 2021). We list the most probable value (i.e., location of maximum \hat{P} of the respective marginalized posterior) and the 68% and 95% confidence intervals (isoproability limits enclosing 68% or 95% of the posterior volume). For comparison, we note that the input (fiducial) reionization history used to generate the data has the optical depth of $\tau = 0.057$, and the start, midpoint, and end of reionization at redshifts 10.36, 7.32, and 5.95, respectively, all of which lie within our 95% confidence intervals.

uncertainties as well as the measurement errors into account, in agreement with Section 2. The IGM contribution is computed based on the true source redshift z^{true} , and using the reionization history from Kulkarni et al. (2019), compatible with current observational constraints on the EoR, and the cosmological parameter values $\Omega_m = 0.3144$, $\Omega_b = 0.04938$, and $H_0 = 67.32 \text{ km s}^{-1} \text{ Mpc}^{-1}$, compatible with Planck (Planck Collaboration et al. 2020). We point out that these inputs are only used to generate the synthetic data sets. Our inference procedure, which is described in Sections 4 and 5, is completely blind to both the cosmological parameters and the input EoR history.

To check that our conclusions do not depend on the specific realization of the synthetic data, we re-run the analysis with two more random realizations of redshift and DM samples. Naturally, the exact numerical values vary from one realization to another (with the strongest impact coming from the number of FRBs observed at $z > 10$), but all runs give comparable constraints and posterior bounds consistent with the true (input) value. In 18 out of 24 computed quantities (eight per run, as in Table 1) the true (input) value lies within the 68% confidence interval, and in all cases lies within the 95% interval.

4. Parameterization of the EoR History

For either a synthetic or a real sample of high-redshift FRBs, the relation between the measured z^{obs} and DM^{obs} depends on the (a priori unknown) values of the cosmological parameters Ω_b , Ω_m , H_0 and, crucially, on the full shape of the reionization history, $x_i(z)$, via the IGM contribution to DM. Therefore, these quantities can be extracted from a sample of high-redshift FRBs. In order to build an inference pipeline, which we describe in Section 5, we, first, need to create a parameterization of the theoretical dispersion measure, $\text{DM}^{\text{model}}(\theta, z')$ following Equations (1) to (4), as a function of the true redshift of the source, z' , and a vector of model parameters θ , which includes the cosmological parameters and the full information about the EoR.

The theoretical dependence of the dispersion measure on the cosmological parameters can straightforwardly be included in the analysis. We take Gaussian priors on the parameters

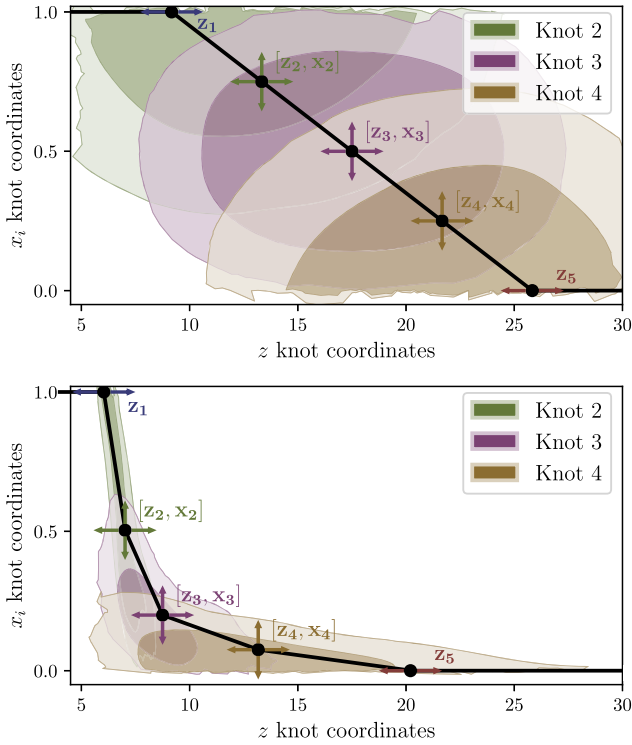


Figure 2. FlexKnot reionization history with $N = 5$ knots, parameterized by the coordinates of the interpolation knots $[z_1, x_{i,1} = 1]$, $[z_2, x_{i,2}]$, $[z_3, x_{i,3}]$, $[z_4, x_{i,4}]$, $[z_5, x_{i,5} = 0]$. The points connected by the solid line show the knots and interpolated FlexKnot reionization history; the arrows indicate the possible movement of the knots. The contours show the positions (for $N = 5$, 1000 FRBs) of the intermediate knots, showing how the knots move from priors (upper panel) to the posteriors (lower panel). Note that the knots tend to cluster at lower redshifts, in the posterior. This is due to a larger variation of $x_i(z)$ as well as more FRBs being observed at lower redshifts. The knots can more precisely constrain the shape of reionization if they are located at low z .

$\Omega_b H_0 = 3.31 \pm 0.017$ and $\Omega_m = 0.311 \pm 0.0056$, based on Planck Collaboration 2020. However, expressing the dependence of $\text{DM}^{\text{model}}(\theta, z')$ on $x_i(z)$ is a more challenging task, as we have to avoid introducing a specific functional form or model.⁶ To this end we use a modified version of the free-form FlexKnot method (Vázquez et al. 2012; Millea & Bouchet 2018).

The FlexKnot method allows us to scan the space of all possible theoretical EoR histories by parameterizing the ionized fraction with N points (referred to as “knots”); Figure 2 shows an example for $N = 5$. These knots can move in order to explore a wide range of plausible reionization histories and determine which histories are compatible with data (either synthetic, as in our case, or future real observations). Each knot is parameterized by a parameter pair $[z_n, x_{i,n}]$ corresponding to its redshift and the value of the ionized fraction at this redshift. Both of these parameters are varied, thus allowing the knot to move freely, in both, z and x_i . This typically leads to most knots moving toward lower redshifts where $x_i(z)$ varies more strongly to achieve a better fit. The reionization history $x_i(z)$ at any arbitrary redshift is then given by the linear interpolation between these knots (Handley et al. 2019), as illustrated in Figure 2 (solid line). In principle, knots can assume any value, but here we require the reionization history to be monotonic, such that the IGM can only become more ionized with time. We also require the first knot (at the lowest redshift) to assume the value of $x_{i,1} = 1$, thus

⁶ Choosing specific functional forms would lead to biases in the results, as discussed in Section 1 and illustrated in Section 6.2.

requiring reionization to be completed by z_1 , and the last knot to have $x_{i,N} = 0$, implying that the universe is still fully neutral at z_N . We allow the redshift locations of the knots to assume any positions consistent with observations; that is, reionization has to be completed by $z = 5$ (McGreer et al. 2015) and begin no earlier than $z = 30$ (as the first stellar populations are expected to form then; e.g., Klessen 2019).

In principle, other model-independent techniques, such as principal component analysis (PCA; Hu & Holder 2003; Heinrich & Hu 2018) or interpolation between values at fixed redshifts (*Poly-reion*; Hazra & Smoot 2017), could be used to parameterize the EoR history instead of the FlexKnot method. What makes FlexKnot stand out compared to the other techniques is not only that both the redshifts and the ionized fractions of the knots are free to vary, but also that the number of knots N is a free parameter. This is equivalent to combining models with different numbers of knots N and weighing them by their Bayesian evidence. High values of N allow the fit to adapt to arbitrarily complex EoR histories while, at the same time, histories with more knots (higher N) than warranted by the data will be downweighted by lower Bayesian evidence.

By design, weighing with respect to Bayesian evidence introduces a slight preference toward simpler reionization histories described with fewer interpolation knots (and, thus, having less variation in the slope). For example, if the data mostly consist of low-redshift FRBs with almost no high-redshift sources, then the strongest constraints on the ionization history are at low redshifts. Such data could be compatible with either a simple late reionization history that happens entirely within the redshift range probed by the FRBs, or with a history that has a small high-redshift tail in the redshift range that is not constrained by the data. Because the former model is simpler (i.e., it requires fewer knots and parameters to describe), it is preferred by the algorithm. As we will see in Section 6.1 this preference for simpler models is not a problem in practice. Even when the maximum posterior indicates a late reionization, the confidence intervals allow for a wider range of reionization histories, including the ones that are more complicated.

5. Parameter Inference

In this section we describe the inference pipeline that is used to constrain reionization history as well as those cosmological parameters that affect the dispersion measure of FRBs.

For a given set of model parameters θ , including the FlexKnot parameters $[z_n, x_{i,n}]$ for knots $n = 1..N$ and the cosmological parameters $\Omega_b H_0$ and Ω_m , we can calculate the theoretical dispersion measure relation, $\text{DM}^{\text{model}}(\theta, z')$, as a function of z' . We compare this model to a set of observations, $d_i = \{\text{DM}_i^{\text{obs}}, z_i^{\text{obs}}\}$, taken from the synthetic catalogs (Section 3). The likelihood of observing the i th FRB from a source at true redshift z' with the expected dispersion measure $\text{DM}^{\text{model}}(\theta, z')$ is

$$P(d_i | \theta, z') = \mathcal{N}\left(\frac{z_i^{\text{obs}} - z'}{\sigma_z(z')}\right) \quad (8)$$

$$\times \mathcal{N}\left(\frac{\text{DM}_i^{\text{obs}} - \text{DM}^{\text{model}}(\theta, z')}{\sigma_{\text{DM}}(z', \text{DM}^{\text{model}}(\theta, z'))}\right), \quad (9)$$

where we assumed normal distributions for the uncertainties in both the redshift and DM. Next, we marginalize over the true source redshift z' , averaging over possible values weighted by

the likelihood and its prior probability distribution, $P(z')$, which we assume to be $P(z') = ze^{-z}$ (Zhou et al. 2014).⁷ Finally, we multiply the independent FRB observations to obtain the likelihood for the entire data set $D = \{d_i\}$:

$$P(D|\theta) = \prod_i \int P(d_i|\theta, z')P(z') dz'. \quad (10)$$

We use the nested sampling (Skilling 2004) algorithm to derive the posterior distributions of both, the cosmological parameters and the reionization history. We sample these parameters assuming flat priors on the positions of the N knots $[z_n, x_{i,n}]$ (between 5 and 30, and 0 and 1, respectively), and Gaussian priors on the cosmological parameters $\Omega_b H_0 = 3.31 \pm 0.017$ and $\Omega_m = 0.311 \pm 0.0056$, based on Planck. Note that these Planck priors do not influence the τ -posterior.

The uniform FlexKnot priors imply nonuniform priors on derived parameters such as the midpoint of reionization z_{mid} or the optical depth τ (Millea & Bouchet 2018). When deriving constraints on these parameters we correct for this effect using maximum entropy priors (following Handley & Millea 2019).

The number of knots, N , is a free parameter in our method. We use a simple implementation, running the nested sampling algorithm individually for each value of N and then combining the runs. This method is equivalent to varying N and all parameters simultaneously. In total we run ten FlexKnot models, from $N=2$ knots (with only beginning and end of reionization defined) to $N_{\text{max}} = 11$. We do not consider more complex models for this data set as for $N \geq 11$ the evidence is small (less than 1% of maximum evidence), and the effect on the results is negligible. We find that, in the case of just 100 FRBs, the simplest model (two knots) has the highest evidence $Z_1 = 1 \pm 0.24$ with three- and four-knot models yielding lower evidence, $Z_3 = 0.57 \pm 0.13$ and $Z_4 = 0.35 \pm 0.08$, respectively. For 1000 FRBs, models with four knots achieve the highest evidence.

The FlexKnot method is very versatile and could easily allow us to incorporate additional constraints on the EoR history from the CMB data by taking into account the effect of $x_i(z)$ on the CMB power spectrum, as well as from other tracers (such as quasars, McGreer et al. 2015, however, adding such constraints is beyond the scope of this paper). Here, as a proof of concept, we make use of this flexibility by adding the constraint on the contribution of the high-redshift universe between $z = 15$ and 30 to the total optical depth, $\tau_{15,30} < 0.019$ (95% confidence; Heinrich & Hu 2021). Note the differentiation between the total τ constraint, and the partial $\tau_{15,30}$ limit: as the CMB experiments are more sensitive to ionization at high redshift, constraints on $\tau_{15,30}$ can be derived in addition to the total τ constraint (see, e.g., Heinrich & Hu 2018; Millea & Bouchet 2018; Planck Collaboration et al. 2020, for similar recent constraints).

6. Results

Finally we apply our method to the synthetic FRB data sets. We make use of the flexibility of the FlexKnot method, which provides the complete reionization history for every sample of

parameters, to derive constraints on some of the characteristic stages of reionization as well as on cosmological parameters τ and A_s .

6.1. Reionization History

We first focus on reionization history and demonstrate that strong constraints on the evolution of the ionized fraction with redshift, $x_i(z)$, can be achieved. To this end, we marginalize individual knot positions and the relevant cosmological parameters (density parameter of matter Ω_m and baryons Ω_b , and the Hubble constant H_0). We find that 1000 FRBs provide good constraints on the shape of reionization history parameterized with four interpolation knots (maximum evidence at $N=4$), while the smaller 100 FRB data set is less sensitive to the details (maximum evidence for the simple $N=2$ model).

The constraints on the ionized fraction $x_i(z)$ obtained from 1000 FRB observations, and additionally using the constraint on $\tau_{15,30}$, are demonstrated in Figure 3. The posterior and prior distributions of $x_i(z)$ are shown by the orange and purple contours, respectively, with 68% and 95% confidence intervals marked by the solid lines. The prior distribution follows from assuming a monotonic reionization history and imposing a uniform prior on each individual knot position. This leads to a weak, nonuniform, prior to the interpolated value of $x_i(z)$ at any given redshift, as indicated by the contours. The posterior provides tight constraints on the reionization history and encompasses the input reionization history that was used to generate the data (dashed cyan line in the figure) within the 95% confidence intervals.

The synthetic FRB data can constrain the reionization history especially well at $z \lesssim 10$ where the vast majority (97%) of the FRB sources in our catalogs are located. The fact that there is only a small number of FRBs at higher redshifts (owing to the steep drop in the adopted SFR, with no FRBs beyond $z > 14$) results in a weaker constraint at $z = 10 - 30$. The high- z constraints are, to a large part, driven by (i) the enforced monotonicity of the function, (ii) the preference for a simpler function (“Occam’s razor,” models with fewer knots are preferred in the Bayesian modeling, provided they can fit the data equally well), and (iii) by the CMB constraint on early reionization via $\tau_{15,30}$.

Based on the FlexKnot samples, we can compute posterior probability distributions for any derived quantity related to the reionization history. Here we choose to constrain the redshifts of the start ($x_i = 0.1$), midpoint ($x_i = 0.5$), and end ($x_i = 0.9$) of reionization. The bounds on these characteristic redshifts are computed in postprocessing and this calculation does not affect other parts of the analysis (such as the derivation of constraints on τ , which we discuss below). The redshift constraints are shown in Figure 3 (blue error bars) with the error bars indicating 68% and 95% confidence limits relative to the peak of the posterior distribution, \hat{P} .⁸ The results are also summarized in Table 1. With 100 FRBs we constrain the end, midpoint, and start of reionization to an accuracy of 7%, 4%, and 11%, respectively (at 68% confidence level). The

⁷ In our calculation we adopted $P(z')$ from Zhou et al. (2014). However, in reality this probability is unknown. We can quantify the error introduced by using an approximate prior as we know the actual redshift distribution of the synthetic data (it follows the SFR). We find that the difference between using the true redshift prior (proportional to SFR) and the approximation (Zhou et al. 2014) is small compared to other contributions, e.g., the resulting error in the value of the CMB optical depth is only $\Delta\tau \lesssim 2\%$.

⁸ The shift seen in Figure 3, between the constraints on characteristic EoR points (blue error bars) and the posterior distribution of reionization histories (orange contours) is expected in our analysis. The orange posterior distribution is subject to the FlexKnot priors (purple), while the blue error bars are prior-corrected as explained in Section 5. The EoR parameters in Table 1 are each corrected with respect to a flat prior, too.

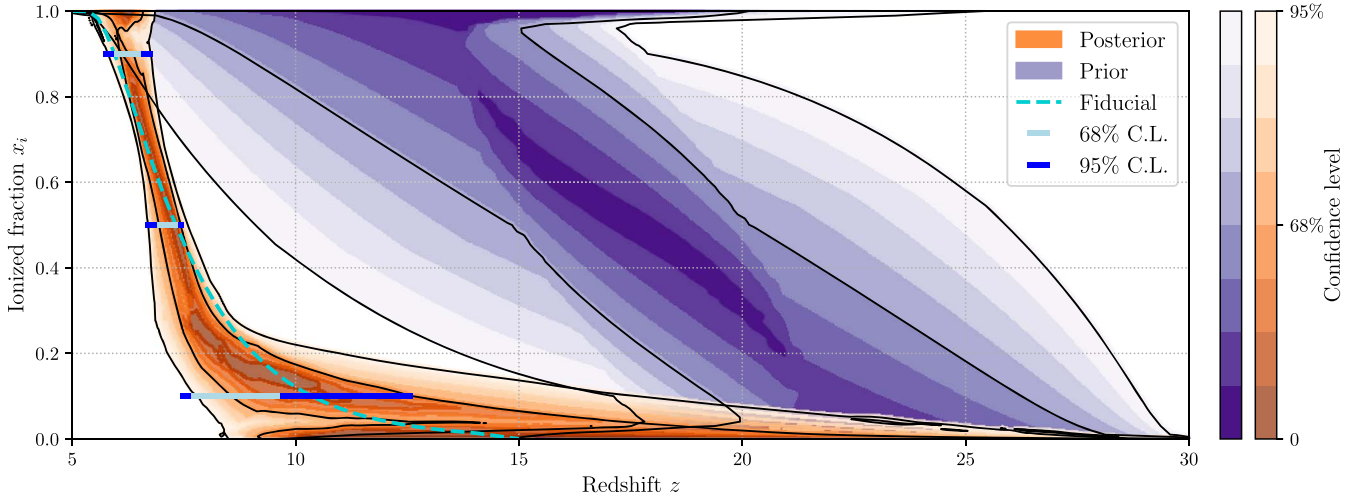


Figure 3. FRB constraints on the full reionization history. We show the posterior (orange) and prior (purple) contours of the reionization history $x_i(z)$ derived from 1000 localized FRBs and including the additional constraint $\tau_{15,30} < 0.019$ (Heinrich & Hu 2021). The constraints are shown as isoprobability contours for $x_i(z)$ at any given redshift, with the confidence level indicated by the color (see colorbars), with 68% and 95% confidence contours marked as solid lines. Additionally, the error bars show the uncertainties in the redshifts of start ($x_i = 0.1$), midpoint ($x_i = 0.5$), and end of reionization ($x_i = 0.9$) as 68% (light blue) and 95% (dark blue) confidence intervals. The dashed cyan line indicates the input (fiducial) reionization history (adopted from Kulkarni et al. 2019) that was used to generate the synthetic FRB data.

corresponding constraints obtained with 1000 FRBs are tighter at lower redshifts, i.e., for the end and the midpoint of reionization, being 5% and 3%, respectively. However, the constraint on the start of the EoR is poor (12%) and is not improved with the sample size. This is because, due to the scarceness of the highest redshift FRBs in our synthetic data, the uncertainties on the start of reionization are highly asymmetric, and the high-redshift tail of the EoR is poorly constrained.

It is illustrative to compare the predicted FRB constraints of the EoR to the present-day state-of-the-art limits. Existing reionization constraints are largely based on quasar and CMB observations. For example, a comprehensive analysis using physical reionization history models (e.g., Greig & Mesinger 2017) shows that the dark fraction of Lyman α and β forest observations, combined with Planck measurements, can constrain the midpoint of reionization to $\sim 12\%$ (at 68% confidence level). Comparing to the forecast for FRBs presented in this paper, we see that even 100 FRBs at $5 < z < 15$ could significantly improve observational constraints on the EoR history, given the redshift distribution and levels of uncertainties assumed here.

6.2. Optical Depth

Using the FRB samples we can also derive constraints on the optical depth τ , marginalizing all possible EoR histories and the relevant cosmological parameters. We derive the posterior probability distribution for τ assuming 100 and 1000 FRBs (shown in Figure 4) and list the detailed limits in Table 1. We find that 100 and 1000 FRBs can constrain the optical depth to 11% and 9% accuracy, respectively (at 68% confidence level; note, however, the asymmetric uncertainties in τ). The precision is comparable to the optical depth measurement of $\tau = 0.0504^{+0.0050}_{-0.0079}$ (13% accuracy, at 68% confidence) derived by the Planck collaboration using a FlexKnot analysis. However, owing to the asymmetric uncertainties in τ resulting from our FRBs analysis, we find that FRBs provide a much stronger lower limit on τ than Planck, while their upper bound

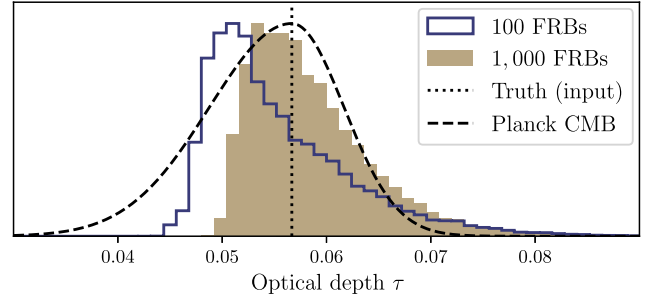


Figure 4. Posterior constraints on the total optical depth τ , marginalized over reionization histories as well as cosmological parameters $\Omega_b \cdot H_0$ and Ω_m . Here we show the constraints from 100 and 1000 FRBs, both including the $\tau_{15,30}$ limit. We compare the constraints to the full Planck FlexKnot measurement $\tau = 0.0504^{+0.0050}_{-0.0079}$ (68% confidence, black dashed line). Note that for the ease of comparison we shifted the Planck posterior distribution to align its mean with our input history. We see that FRBs can significantly improve the lower limit on the total optical depth constraint.

is weaker due to the low SFR at high redshifts. This behavior also persists if we remove the $\tau_{15,30}$ constraint (last row of Table 1), and the lower bounds on τ stay at nearly the same values.

To explore the origin of the asymmetric optical depth constraints, we consider the contributions of low, $\tau_{z < 10}$, and high, $\tau_{z > 10}$, redshift to τ separately. For the former we find a tight constraint that improves with the data size, with the uncertainty (at 68% confidence level) decreasing from 5% for 100 to 2% for 1000 FRBs.⁹ For the high-redshift contribution, $\tau_{z > 10}$, we can only obtain upper limits and find $\tau_{z > 10} < 0.0049$ for 100 FRBs and $\tau_{z > 10} < 0.0071$ for 1000 FRBs at 68% confidence. These upper limits are compatible with the true value $\tau_{z > 10} = 0.0024$, but do not yield stringent constraints for either data set. The expected scarcity of the high-redshift FRBs leading to the weak constraints on the high-redshift contribution to τ is the main limiting factor in precision τ measurement with FRBs. However, as this contribution cannot

⁹ More precisely the constraints are $\tau_{z < 10} = 0.0508^{+0.0027}_{-0.0023}$ for the sample of 100 FRBs and $\tau_{z < 10} = 0.0528^{+0.0011}_{-0.0011}$ for 1000 FRBs.

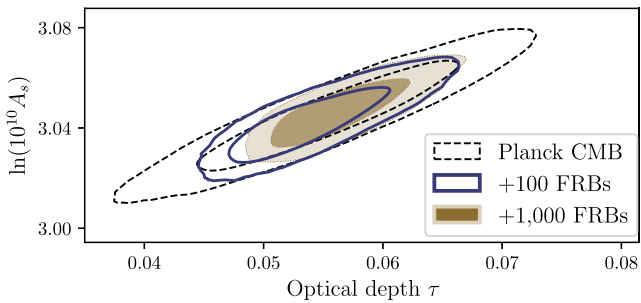


Figure 5. 2D posterior constraints on the primordial power spectrum amplitude A_s and the optical depth τ . Compared to the [Planck](#) constraints, adding τ constraints from FRBs significantly decreases the uncertainty in A_s . 100 or 1000 FRBs would allow constraints of $\ln(10^{10}A_s) = 3.041^{+0.011}_{-0.009}$ or $\ln(10^{10}A_s) = 3.047^{+0.010}_{-0.007}$, respectively, compared to the [Planck](#) constraint of $\ln(10^{10}A_s) = 3.043^{+0.016}_{-0.012}$ (68% confidence intervals).

be negative, it barely affects the lower bound on τ thus allowing to derive stringent lower limits.

As mentioned in Section 1, the FlexKnot method can give more accurate FRB EoR constraints than the common fixed-shape techniques. As a specific example, we consider the popular tanh parameterization (used, e.g., in Zhang et al. 2021), applied to our synthetic data set. Sampling its two parameters (redshift of reionization z_{reio} and width Δz) yields a posterior constraint on the optical depth $\tau_{\text{tanh}} = 0.0494^{+0.0030}_{-0.0013}$ (68% confidence) for 100 FRBs and $\tau_{\text{tanh}} = 0.0514^{+0.0014}_{-0.0006}$ for 1000 FRBs. These inferences systematically underestimate the true optical depth ($\tau = 0.057$) by about 10% at a high statistical significance: The 100 and 1000 FRB tanh posteriors exclude the true value at $>95\%$ and $>99.7\%$ confidence level, respectively, while the FlexKnot results for the same data (Table 1) remain consistent with the input at 68% confidence level. The reason for this difference lies in the shape of the tanh history, which does not match that of the input reionization history (Kulkarni et al. 2019). In a real-life situation the magnitude of this effect will, of course, depend on how close the actual (unknown) EoR history is to the assumed parameterization. There is no way of testing the effect size beforehand and, thus, we suggest using a free-form method like FlexKnot to avoid this problem altogether.

6.3. Cosmological Implications of Tight τ Constraints from FRBs

An accurate optical depth measurement is not only useful as a probe of reionization, but it will also improve the cosmological constraints achievable with other experiments. As an example, Figure 5 shows the marginalized two-dimensional constraints on τ and the initial amplitude of curvature perturbations, A_s , as measured by [Planck](#) (dashed contour lines; from the [Planck Legacy Archive](#)¹⁰), which are well known to be degenerate with τ (Hazra et al. 2018). An independent optical depth measurement from FRBs allows for tighter constraints on A_s (solid and filled contours in Figure 5). We find that adding the constraints on τ from 100 or 1000 FRBs to the [Planck](#) data reduces relative error in $\ln(10^{10}A_s)$ from 0.46% to 0.32% and 0.29%, respectively.

¹⁰ Full chains for parameter results from https://pla.esac.esa.int/pla/COM_CosmoParams_fullGrid_R3_01 using CMB power spectra, lensing, and Baryonic Acoustic Oscillations.

Tighter reionization constraints also improve limits on the sum of neutrino masses, Σm_ν . Future large-scale structure surveys such as DESI (DESI Collaboration et al. 2016), Euclid (Amendola et al. 2018), and SKA,¹¹ as well as ground-based CMB telescopes (such as CMB-S4; Abazajian et al. 2016), aim to measure Σm_ν but can only achieve their full potential in combination with an independent optical depth measurement as demonstrated by Brinckmann et al. (2019). They show that CMB-S4 + Euclid can only detect neutrino masses deviating from zero with a strong lower limit on τ . Thus an optical depth constraint from FRBs could significantly contribute to a cosmological detection of the sum of neutrino masses, and in combination with constraints from large-scale CMB polarization measurements (e.g., from LiteBIRD; Matsumura et al. 2014), FRBs can improve the precision of Σm_ν measurements.

7. Conclusion

In this work we explore the potential of high-redshift FRBs to improve our understanding of the universe by providing new, independent, constraints on the reionization history. Our analysis is unique in that it is based on a free-form FlexKnot technique and, thus, the results are not influenced by assumptions about the reionization history. This is in contrast to some of the previous works on this topic where a specific shape of the reionization history was postulated.

Using synthetic FRB data, distributed at $z = 5\text{--}15$ according to the star formation rate, we show that the full shape of reionization history can be accurately extracted from the dispersion measures of such localized high-redshift events. We find that even a sample of 100 localized FRBs at $z > 5$ will allow us to improve reionization constraints beyond the current state-of-the-art CMB bounds and limits derived from high-redshift quasars. A sample of 1000 FRBs provides tight constraints of 5%, 3%, and 12% on the end, midpoint, and start of reionization, respectively (corresponding results for 100 localized FRBs are also quoted in Section 6).

The flexibility of the FlexKnot method allows us to marginalize over reionization histories and derive model-independent bounds on the CMB optical depth τ . FRBs could improve current limits on τ and, through it, on other cosmological parameters such as the sum of neutrino masses and the amplitude of the power spectrum of primordial fluctuations A_s . We show that even 100 FRBs can constrain τ to an accuracy of 11% (at a 68% confidence level), which is better than the constraints derived from the [Planck](#) FlexKnot analysis ($\sim 13\%$). Owing to the higher numbers of FRBs at lower redshifts, the τ constraints are asymmetric with a much stronger lower limit of 7% (at 68% confidence level). Next, we find that the independent constraints on reionization from 100 FRBs reduce relative error in $\ln(10^{10}A_s)$ from 0.46% to 0.32% when added to the [Planck](#) data. The tight lower limit on τ will help constrain the sum of neutrino masses from below, potentially contributing to a cosmological detection of the neutrino mass.

Finally, we note that measuring the overall amplitude of the DM(z) relation at high redshifts could, in principle, allow us to constrain other cosmological parameters as well since the amplitude is proportional to the combination $\Omega_b H_0 \Omega_m^{-0.5}$. However, we do not focus on such constraints here because these parameters can be constrained by the low-redshift ($z < 5$)

¹¹ <https://www.skatelescope.org/>

FRB data to a much greater accuracy (Zhou et al. 2014; Hagstotz et al. 2022).

In summary, a successful high- z FRB survey could substantially advance our understanding of reionization and provide powerful new constraints on cosmological parameters.

We thank A. Boyle, S. Gratton, M. Haehnelt, W. Handley, and L. Hergt for helpful discussions. We also thank the anonymous referee for their comments and suggestions that helped improve our paper. We acknowledge the usage of the DiRAC HPC. A.F. was supported by the Royal Society University Research Fellowship. N.S.S. was funded by the URF Enhancement Award of A.F. D.R.L. acknowledges support from NSF awards AAG-1616042, OIA-1458952, and PHY-1430284. S.H. acknowledges the support of STFC, via the award of a DTP Ph.D. studentship, and the Institute of Astronomy for a maintenance award.

Tools and Data Availability

In the interest of reproducibility and to facilitate the usage of this method, we make our source code and data publicly available (data and codes in Heimersheim et al. 2021, and updated codes on GitHub).¹²

We sample the posterior parameter spaces using the PolyChord code (Handley et al. 2015a, 2015b) and the cobaya wrapper (Torrado & Lewis 2019, 2021). We visualize these distributions using the analysis codes fgivenx (functional posterior, Handley 2018) and anesthetic (contour plots, Handley 2019). The codes make extensive use of the astropy (Astropy Collaboration et al. 2013, 2018), scipy (Virtanen et al. 2020), and numpy (Harris et al. 2020) python libraries.

ORCID iDs

Stefan Heimersheim  <https://orcid.org/0000-0001-9631-4212>

Nina S. Sartorio  <https://orcid.org/0000-0003-2138-5192>

Anastasia Fialkov  <https://orcid.org/0000-0002-1369-633X>

Duncan R. Lorimer  <https://orcid.org/0000-0003-1301-966X>

References

- Abazajian, K. N., Adshead, P., Ahmed, Z., et al. 2016, arXiv:1610.02743
- Agarwal, D., Lorimer, D. R., Surnis, M. P., et al. 2020, *MNRAS*, 497, 352
- Amendola, L., Appleby, S., Avgoustidis, A., et al. 2018, *LRR*, 21, 2
- Arcus, W. R., Macquart, J. P., Sammons, M. W., James, C. W., & Ekers, R. D. 2021, *MNRAS*, 501, 5319
- Astropy Collaboration, Price-Whelan, A. M., & Sipőcz, B. M. 2018, *AJ*, 156, 123
- Astropy Collaboration, Robitaille, T. P., Tollerud, E. J., et al. 2013, *A&A*, 558, A33
- Bannister, K. W., Deller, A. T., Phillips, C., et al. 2019, *Sci*, 365, 565
- Batten, A. J., Duffy, A. R., Wijers, N. A., et al. 2021, *MNRAS*, 505, 5356
- Behroozi, P., Wechsler, R. H., Hearin, A. P., & Conroy, C. 2019, *MNRAS*, 488, 3143
- Beniamini, P., Kumar, P., Ma, X., & Quataert, E. 2021, *MNRAS*, 502, 5134
- Bhandari, S., Keane, E. F., Barr, E. D., et al. 2018, *MNRAS*, 475, 1427
- Bhattacharya, M., Kumar, P., & Linder, E. V. 2021, *PhRvD*, 103, 103526
- Bochenek, C. D., Ravi, V., Belov, K. V., et al. 2020, *Natur*, 587, 59
- Brinckmann, T., Hooper, D. C., Archidiacono, M., Lesgourgues, J., & Sprenger, T. 2019, *JCAP*, 2019, 059
- Condon, J. J., & Ransom, S. M. 2016, *Essential Radio Astronomy* (Princeton, NJ: Princeton Univ. Press)
- Cordes, J. M., & Lazio, T. J. W. 2002, arXiv:astro-ph/0207156
- Dai, J.-P., & Xia, J.-Q. 2021, *JCAP*, 2021, 050
- Das, S., Mathur, S., Gupta, A., Nicastro, F., & Krongold, Y. 2021, *MNRAS*, 500, 655
- Deng, W., & Zhang, B. 2014, *ApJL*, 783, L35
- DESI Collaboration, Aghamousa, A., Aguilar, J., et al. 2016, arXiv:1611.00036
- Fialkov, A., & Loeb, A. 2016, *JCAP*, 2016, 004
- Fialkov, A., & Loeb, A. 2017, *ApJL*, 846, L27
- Gao, H., Li, Z., & Zhang, B. 2014, *ApJ*, 788, 189
- Greig, B., & Mesinger, A. 2017, *MNRAS*, 465, 4838
- Hagstotz, S., Reischke, R., & Lilow, R. 2022, *MNRAS*, 511, 662
- Handley, W. 2018, *JOSS*, 3, 849
- Handley, W. 2019, *JOSS*, 4, 1414
- Handley, W., & Millea, M. 2019, *Entrp*, 21, 272
- Handley, W. J., Hobson, M. P., & Lasenby, A. N. 2015a, *MNRAS*, 450, L61
- Handley, W. J., Hobson, M. P., & Lasenby, A. N. 2015b, *MNRAS*, 453, 4384
- Handley, W. J., Lasenby, A. N., Peiris, H. V., & Hobson, M. P. 2019, *PhRvD*, 100, 103511
- Harris, C. R., Millman, K. J., van der Walt, S. J., et al. 2020, *Natur*, 585, 357
- Hashimoto, T., Goto, T., Lu, T.-Y., et al. 2021, *MNRAS*, 502, 2346
- Hashimoto, T., Goto, T., On, A. Y. L., et al. 2020a, *MNRAS*, 497, 4107
- Hashimoto, T., Goto, T., On, A. Y. L., et al. 2020b, *MNRAS*, 498, 3927
- Hashimoto, T., Laporte, N., Mawatari, K., et al. 2018, *Natur*, 557, 392
- Hazra, D. K., Paoletti, D., Finelli, F., & Smoot, G. F. 2018, *JCAP*, 2018, 016
- Hazra, D. K., & Smoot, G. F. 2017, *JCAP*, 2017, 028
- Heimersheim, S., Sartorio, N. S., Fialkov, A., & Lorimer, D. R. 2021, Data and Code for “What it Takes to Measure Reionization with Fast Radio Bursts”, Zenodo, doi:10.5281/zenodo.6542596
- Heinrich, C., & Hu, W. 2018, *PhRvD*, 98, 063514
- Heinrich, C., & Hu, W. 2021, *PhRvD*, 104, 063505
- Hu, W., & Holder, G. P. 2003, *PhRvD*, 68, 023001
- James, C. W., Prochaska, J. X., Macquart, J. P., et al. 2022, *MNRAS*, 510, L18
- Jaroszynski, M. 2019, *MNRAS*, 484, 1637
- Jaroszynski, M. 2020, *AcA*, 70, 87
- Keating, L. C., & Pen, U.-L. 2020, *MNRAS*, 496, L106
- Klessen, R. 2019, in *Formation of the First Stars*, ed. M. Latif & D. Schleicher (Singapore: World Scientific), 67
- Kulkarni, G., Keating, L. C., Haehnelt, M. G., et al. 2019, *MNRAS*, 485, L24
- Kulkarni, S. R. 2020, arXiv:2007.02886
- Kumar, P., & Linder, E. V. 2019, *PhRvD*, 100, 083533
- Linder, E. V. 2020, *PhRvD*, 101, 103019
- Lorimer, D. R., Bailes, M., McLaughlin, M. A., Narkevic, D. J., & Crawford, F. 2007, *Sci*, 318, 777
- Lorimer, D. R., Karastergiou, A., McLaughlin, M. A., & Johnston, S. 2013, *MNRAS*, 436, L5
- Macquart, J. P., Prochaska, J. X., McQuinn, M., et al. 2020, *Natur*, 581, 391
- Madhavacheril, M. S., Battaglia, N., Smith, K. M., & Sievers, J. L. 2019, *PhRvD*, 100, 103532
- Matsumura, T., Akiba, Y., Borrill, J., et al. 2014, *JLTP*, 176, 733
- McGreer, I. D., Mesinger, A., & D’Oro, V. 2015, *MNRAS*, 447, 499
- Millea, M., & Bouchet, F. 2018, *A&A*, 617, A96
- Nan, R., Li, D., Jin, C., et al. 2011, *IJMPD*, 20, 989
- Naoz, S., Noter, S., & Barkana, R. 2006, *MNRAS*, 373, L98
- Oesch, P. A., Brammer, G., van Dokkum, P. G., et al. 2016, *ApJ*, 819, 129
- Pagano, M., & Fronenberg, H. 2021, *MNRAS*, 505, 2195
- Petroff, E., Barr, E. D., Jameson, A., et al. 2016, *PASA*, 33, e045
- Planck Collaboration, Aghanim, N., Akrami, Y., et al. 2020, *A&A*, 641, A6
- Popov, S. B., & Postnov, K. A. 2010, in *Evolution of Cosmic Objects through their Physical Activity*, ed. H. A. Harutyunian, A. M. Mickaelian, & Y. Terzian (Yerevan: “Gitutyun” Publishing House of NAS RA), 129, arXiv:0710.2006
- Rafiei-Ravandi, M., Smith, K. M., Li, D., et al. 2021, *ApJ*, 922, 42
- Skilling, J. 2004, in *AIP Conf. Ser. 735, Bayesian Inference and Maximum Entropy Methods in Science and Engineering*, ed. R. Fischer, R. Preuss, & U. V. Toussaint (Melville, NY: AIP), 395
- Takahashi, R., Ioka, K., Mori, A., & Funahashi, K. 2021, *MNRAS*, 502, 2615
- Tendulkar, S. P., Bassa, C. G., Cordes, J. M., et al. 2017, *ApJL*, 834, L7
- The CHIME/FRB Collaboration, Andersen, B. Á. C., Bandura, K. Á. M., et al. 2020, *Natur*, 587, 54
- Torrado, J., & Lewis, A. 2019, *Cobaya: Bayesian Analysis in Cosmology, Astrophysics Source Code Library*, ascl:1910.019
- Torrado, J., & Lewis, A. 2021, *JCAP*, 2021, 057
- Vázquez, J. A., Bridges, M., Hobson, M. P., & Lasenby, A. N. 2012, *JCAP*, 2012, 006
- Virtanen, P., Gommers, R., Oliphant, T. E., et al. 2020, *Nature Methods*, 17, 261
- Wadiasingh, Z., Beniamini, P., Timokhin, A., et al. 2020, *ApJ*, 891, 82

¹² <https://github.com/Stefan-Heimersheim/FlexKnotFRB>

- Walters, A., Ma, Y.-Z., Sievers, J., & Weltman, A. 2019, [PhRvD](#), **100**, 103519
- Walters, A., Weltman, A., Gaensler, B. M., Ma, Y.-Z., & Witzemann, A. 2018, [ApJ](#), **856**, 65
- Wu, Q., Yu, H., & Wang, F. Y. 2020, [ApJ](#), **895**, 33
- Xu, J., & Han, J. L. 2015, [RAA](#), **15**, 1629
- Yamasaki, S., & Totani, T. 2020, [ApJ](#), **888**, 105
- Yang, Y.-P., & Zhang, B. 2016, [ApJL](#), **830**, L31
- Yao, J. M., Manchester, R. N., & Wang, N. 2017, [ApJ](#), **835**, 29
- Zhang, B. 2018, [ApJL](#), **867**, L21
- Zhang, Z. J., Yan, K., Li, C. M., Zhang, G. Q., & Wang, F. Y. 2021, [ApJ](#), **906**, 49
- Zheng, Z., Ofek, E. O., Kulkarni, S. R., Neill, J. D., & Juric, M. 2014, [ApJ](#), **797**, 71
- Zhou, B., Li, X., Wang, T., Fan, Y.-Z., & Wei, D.-M. 2014, [PhRvD](#), **89**, 107303